

NUMERICAL SIMULATION ON LOW-SPEED HYDROGEN JET DIFFUSION

Takatori, Y. ¹, Tsuboi, N. ², Fujimoto, K. ³, Muto, D. ⁴ and Asahara, M. ⁵

¹ Department of Mechanical Engineering, Aoyama Gakuin University, 5-10-1 Fuchinobe, Chuo-ku, Sagamihara, Kanagawa, 229-8558, Japan, tsgfcghrfufc@gmail.com

² Department of Mechanical and Control Engineering, Kyushu Institute of Technology, 1-1 Sensui-chou, Tobata-ku, Kitakyushu, Fukuoka, 804-8550, Japan, tsuboi@mech.kyutech.ac.jp

³ Department of Mechanical and Control Engineering, Kyushu Institute of Technology, 1-1 Sensui-chou, Tobata-ku, Kitakyushu, Fukuoka, 804-8550, Japan, meteor9150@gmail.com

⁴ Department of Mechanical and Control Engineering, Kyushu Institute of Technology, 1-1 Sensui-chou, Tobata-ku, Kitakyushu, Fukuoka, 804-8550, Japan, daiki.muto@gmail.com

⁵ Department of Mechanical Engineering, Aoyama Gakuin University, 5-10-1 Fuchinobe, Chuo-ku, Sagamihara, Kanagawa, 229-8558, Japan, asahara@me.aoyama.ac.jp

ABSTRACT

The numerical simulation for the hydrogen jet experiments performed by Schefer et al., is conducted using the compressible, multicomponent Navier-Stokes equations with the preconditioning method. The simulated results for the hydrogen jet agree with the theoretical results of Tollmien. As far as comparing with the experiments by Schefer et al., the concentration profiles along the radial direction agree with the present numerical results and that along the centerline also agree well with the experimental results after the data are normalized by the equivalent nozzle diameter. It is confirmed that the spread of the jet width from the jet exit to downstream is affected by the Kelvin-Helmholtz instability. It is also confirmed that the jet flow field is formed alternately by the high pressure region and the low pressure one to cause the jet flow fluctuation.

1.0 INTRODUCTION

After fuel cell vehicles become commercially available, a future demand expansion for hydrogen fuel is expected and an installation expansion is prospective in the future. Since hydrogen energy society is prospective in the future, it is necessary to investigate the fundamental properties of hydrogen. Hydrogen is light gas, mostly diffusive in all gases, and flammable and its ignition energy of 0.02 mJ is quite low. The lower flammable limit of hydrogen in air is 4 % in mole fraction and the higher one is 75 % in mole fraction. The detonation limits of hydrogen in air are 18 % at the lower case and 59 % at the higher case, and then it is easy to ignite when hydrogen leaks. Hydrogen is stored as a liquid or as a solid hydride) at a high pressure for the tank of hydrogen station and fuel cell. When the stored hydrogen leaks due to the break of tube, it diffuses out unsteadily at a short time. Then the flammable region of hydrogen/air mixture expands over a wide range. When an ignition source exists in the region of leaked hydrogen, an explosion can happen. Hence in order to predict and to prevent an accident by the hydrogen leaking from the stored tank by any chance, it is necessary to comprehend the dynamics of hydrogen diffusion and to set up an appropriate standard and control for hydrogen properties.

The research on the ignition in jet flow investigated in 1981 by Birch et al. [1] has shown that the calculated mole concentration at the lower flammability limit in a natural gas jet does not agree with that at the lower flammability limit in the static condition. They also reported that it is possible to predict the ignition condition from the average concentration data although the average concentration cannot be related with the ignition limit in the case of combustion. Swain et al. [2,3] showed experimentally that the hydrogen gas concentration near the ignition boundary does not agree with the combustible limit of 4 % under the static condition. They also showed that the ignition condition in the jet depends on the ignition energy of the spark plug and the spark plug gap, that it is difficult to measure the mole concentration accurately at the ignition location, and that the minimum mole concentration at ignition is about 5-10 %. In order to characterize the flammability limits in jets, concentration measurement experiments [4, 5, 6] are performed in

turbulent jets. The concentration measurements are typically performed to get ignition conditions. Schefer et al. [7, 8] showed in the past experiments that the momentum of hydrogen jet under low Froude number conditions is affected by the buoyancy. Especially the effect of the buoyancy is prominent downstream and the concentration fluctuation of hydrogen is strong there. Schefer et al. also showed that the hydrogen jet fluctuation is obtained from the probability density distribution and the hydrogen appearance probability near the centerline of the jet has a Gauss distribution. On the other hand, they reported that the probability density function at the outer edge, where hydrogen and air mix, has a bimodal distribution. The studies on hydrogen jet and combustion are mostly performed experimentally and are scarcely done numerically [9, 10, 11]. The present study will simulate the experiments by Schefer et al. numerically to elucidate the detailed mechanism of a hydrogen jet.

2.0 GOVERNING EQUATIONS

An incompressible flow solution method is generally used to solve a low speed flow numerically. However we will solve a jet flow with combustion reactions using an ignition source in a high pressure hydrogen jet in the near future. The jet spouting with a high pressure becomes a compressible flow with a high Mach number near the nozzle exit. Such a jet becomes an incompressible flow with a low Mach number far from the nozzle exit. Hence, when the high pressure spouting jet is simulated numerically, both the compressible and incompressible flows must be effectively solved at the same time. Further when the jet flow is combustible, it has a density fluctuation as pressure fluctuates largely. Therefore it is essential to consider compressibility in order to capture the pressure fluctuation induced by combustion. It will be a problem that when the incompressible slow speed flow and combustion are mixed with the high pressure compressible flow. There exists a region where the Mach number becomes quite low. In order to solve a compressible flow numerically, the time step is restricted tightly and the convergence of solution becomes worse. Such problem comes from the situation that the large condition number, which consists of the ratio between the maximum and minimum of eigenvalues related with the convective terms of the compressible flow, becomes a cause. The conventional compressible flow solver becomes stiffness and shows a slow convergence as the order of the large condition number is larger than 100. In order to solve the problem of the mix of compressible and incompressible flow, the pre-conditioning method [12, 13, 14, 15] can be applied. Hence the numerical analysis method used in the present study is the three-dimensional compressible Navier-Stokes equations with the pre-conditioning method and with considering incompressibility of the fluid.

The governing equations, the three-dimensional compressible Navier-Stokes equations, consist of the conservation law of mass, momentum, and energy and the species conservation of nine chemical species (H_2 , O_2 , H , O , OH , HO_2 , H_2O_2 , H_2O , N_2). The compressible Navier-Stokes equations described in three-dimensional Cartesian coordinates are:

$$\frac{\partial \mathbf{Q}}{\partial t} + \frac{\partial \mathbf{E}}{\partial x} + \frac{\partial \mathbf{F}}{\partial y} + \frac{\partial \mathbf{G}}{\partial z} = \frac{\partial \mathbf{E}_v}{\partial x} + \frac{\partial \mathbf{F}_v}{\partial y} + \frac{\partial \mathbf{G}_v}{\partial z} \quad (1)$$

$$\mathbf{Q} = \begin{pmatrix} \rho \\ \rho u \\ \rho v \\ \rho w \\ e \\ \rho_1 \\ \vdots \\ \rho_N \end{pmatrix}, \mathbf{E} = \begin{pmatrix} \rho u \\ \rho u^2 + p \\ \rho uv \\ \rho uw \\ (e + p)u \\ \rho_1 u \\ \vdots \\ \rho_N u \end{pmatrix}, \mathbf{F} = \begin{pmatrix} \rho v \\ \rho vu \\ \rho v^2 + p \\ \rho vw \\ (e + p)v \\ \rho_1 v \\ \vdots \\ \rho_N v \end{pmatrix}, \mathbf{G} = \begin{pmatrix} \rho w \\ \rho wu \\ \rho wv \\ \rho w^2 + p \\ (e + p)w \\ \rho_1 w \\ \vdots \\ \rho_N w \end{pmatrix} \quad (2)$$

$$\mathbf{E}_v = \begin{pmatrix} 0 \\ \tau_{xx} \\ \tau_{xy} \\ \tau_{xz} \\ \tau_{xx}u + \tau_{xy}v + \tau_{xz}w - q_x \\ \dot{m}_{x,1} \\ \vdots \\ \dot{m}_{x,N} \end{pmatrix}, \mathbf{F}_v = \begin{pmatrix} 0 \\ \tau_{yx} \\ \tau_{yy} \\ \tau_{yz} \\ \tau_{yx}u + \tau_{yy}v + \tau_{yz}w - q_y \\ \dot{m}_{y,1} \\ \vdots \\ \dot{m}_{y,N} \end{pmatrix}, \mathbf{G}_v = \begin{pmatrix} 0 \\ \tau_{zx} \\ \tau_{zy} \\ \tau_{zz} \\ \tau_{zx}u + \tau_{zy}v + \tau_{zz}w - q_z \\ \dot{m}_{z,1} \\ \vdots \\ \dot{m}_{z,N} \end{pmatrix} \quad (3)$$

where ρ is the density in kg/m^3 , u is the velocity in the x direction, v is the velocity in the y direction, w is the velocity in the z direction in m/s , e is the total energy per specific volume in J/m^3 , i is the index of the chemical species ($i=1, 2, \dots, N$), N is the total number of species, ρ_i is the density of the i th species in kg/m^3 , p is the pressure in Pa, τ is the shearing stress of each component in Pa, q is the heat flux of each direction in W/m^2 , \dot{m} is the diffusion mass flux of the i th species in $\text{kg/m}^2\text{s}$. Q is called the conservation variable vector. Here the unsteady preconditioning method including the multi-species conservation equations is extended based on the Weiss et al. [16] method. Replacing the conservative variable vector Q with the fundamental variable W and using the pre-conditioning matrix Γ give

$$\frac{\partial Q}{\partial t} + \Gamma \frac{\partial W}{\partial \tau} + \frac{\partial E}{\partial x} + \frac{\partial F}{\partial y} + \frac{\partial G}{\partial z} = \frac{\partial E_v}{\partial x} + \frac{\partial F_v}{\partial y} + \frac{\partial G_v}{\partial z} \quad (4)$$

$$W = [p, u, v, w, h, Y_i]^T \quad (5)$$

$$\Gamma = \begin{bmatrix} \Theta & 0 & 0 & 0 & 0 & -\rho \mathfrak{R}_1 & \dots & -\rho \mathfrak{R}_N \\ \Theta u & \rho & 0 & 0 & 0 & -\rho \mathfrak{R}_1 u & \dots & -\rho \mathfrak{R}_N u \\ \Theta v & 0 & \rho & 0 & 0 & -\rho \mathfrak{R}_1 v & \dots & -\rho \mathfrak{R}_N v \\ \Theta w & 0 & 0 & \rho & 0 & -\rho \mathfrak{R}_1 w & \dots & -\rho \mathfrak{R}_N w \\ \Theta H - 1 & \rho u & \rho v & \rho w & \rho & \rho h_1 - \rho \mathfrak{R}_1 H & \dots & \rho h_N - \rho \mathfrak{R}_N H \\ \Theta Y_1 & 0 & 0 & 0 & 0 & -\rho \mathfrak{R}_1 Y_1 + \rho & \dots & -\rho \mathfrak{R}_N Y_1 \\ \vdots & \vdots & \vdots & \vdots & \vdots & \vdots & \ddots & \vdots \\ \Theta Y_N & 0 & 0 & 0 & 0 & -\rho \mathfrak{R}_1 Y_N & \dots & -\rho \mathfrak{R}_N Y_N + \rho \end{bmatrix} \quad (6)$$

$$\mathfrak{R}_i = \frac{R_i}{\sum_{i=1}^N Y_i R_i} \quad (7)$$

$$H = \frac{\bar{h} + (u^2 + v^2 + w^2)}{2} \quad (8)$$

$$\Theta = \frac{1}{U_r^2} - \frac{1}{c^2} + \rho_p \quad (9)$$

where T is the temperature in K, Y_i is the mass fraction of the i th species in %, c is the speed of sound in m/s , R_i is the gas constant of the i th species in $\text{J/(K}\cdot\text{mol)}$, and $U_r = \min[c^2, \max(|V|^2, \varepsilon |V_\infty|^2)]$, respectively. t is real time and τ is pseudo time. The present simulations uses $\varepsilon=0.25$.

Time accuracy assumes second-order and s is the number of sub-iteration, then the Eq. (4) becomes

$$\left[\Gamma + \frac{3\Delta\tau}{2\Delta t} \frac{\partial Q}{\partial W} \right] \Delta W^{(s)} = -\Delta\tau \left[RHS^{(s-1)} + \frac{3Q^{(s-1)} - 4Q^n + Q^{n-1}}{2\Delta t} \right] \quad (10)$$

3.0 NUMERICAL METHODS

The inviscid flux adopts the preconditioning AUSMDV[17]. The second-order MUSCL without limiter is used. The viscous term is second-order central difference. Time integration uses preconditioned Euler explicit method because the computational cost for third-order preconditioned TVD Runge-Kutta method is three times more than that for preconditioned Euler explicit method. The number of sub-iteration is set as 10 times in order to preserve time accuracy. Turbulent model is not used in this simulation due to low Reynolds number although the resolution study and turbulent model effects should be estimated in the future.

4.0 NUMERICAL CONDITIONS

The numerical grid system is described in Fig. 1. The nozzle exit width d is 19.1 mm. The x -direction length x/d is 100. The y -direction height y/d is 150. The z -direction length is 2.35 mm. The numbers of the grid system are 121 points in x -direction, 111 points in y -direction, and 5 points in z -direction. Therefore, the present simulation uses planar grid system because the computer code is constructed for three-dimensional grid system. The total number of the grids is about 67,000 points. The minimum grid size is $\Delta x = \Delta y = \Delta z = 477 \mu\text{m}$. The grid points are set closer together in the boundary region near the nozzle exit and are arranged widely near the other boundaries since the flow field can be changed by the effect of the boundary conditions.

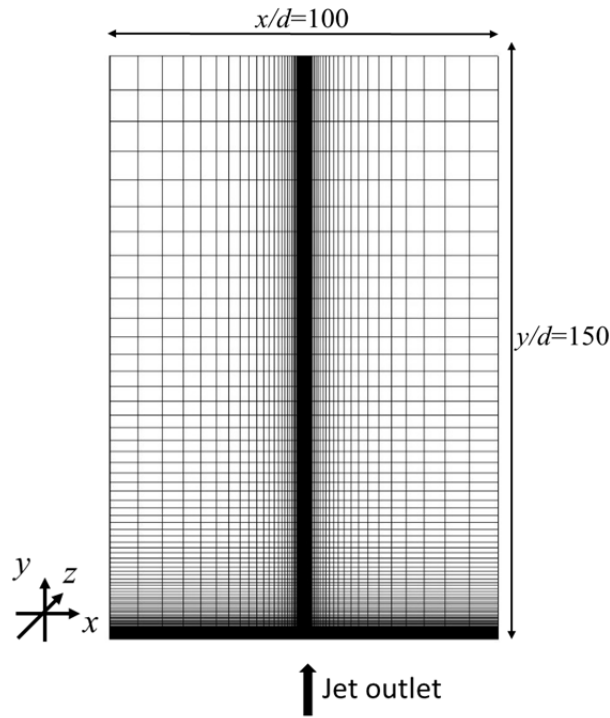


Figure 1. Numerical grid for low-speed hydrogen jet.

The initial conditions set for the gas are shown in Table 1. Jet gas is H_2 , with an initial density ρ_j of 0.082 kg/m^3 , an initial temperature T_j of 300 K, an initial pressure P_j of 0.1 MPa, an initial velocity u_j of 134 m/s, and an initial Mach number of 0.106. The jet sets uniform distributions. Ambient gas is air (mass fractions of O_2 and N_2 are 0.244 and 0.756), with an initial density ρ_0 of 1.177 kg/m^3 , an initial temperature T_0 of 300 K, an initial pressure P_0 of 0.1 MPa, an initial velocity u_0 of 134 m/s and an initial Mach number of 0.

Table 1. Numerical conditions.

	Outlet	Ambient
Mixture Gas	H ₂	Air (O ₂ :N ₂ = 0.244:0.756)
Density	$\rho_i = 0.082 \text{ kg/m}^3$	$\rho_0 = 1.177 \text{ kg/m}^3$
Temperature	$T_i = 300 \text{ K}$	$T_0 = 300 \text{ K}$
Pressure	$P_i = 0.1 \text{ MPa}$	$P_0 = 0.1 \text{ MPa}$
Velocity	$u_i = 134 \text{ m/s}$	$u_0 = 0 \text{ m/s}$
Mach number	0.106	0

5.0 RESULTS AND DISCUSION

5.1 Program Validation

Figure 2(a) shows the average Mach number profiles and Figure 2(b) shows the comparison of the non-dimensional numerical radial velocity profiles with the non-dimensional analytical radial velocity profile using the Tollmien axisymmetric jet flow theory at the x -axis locations of $y/d=10.1, 12.7,$ and 14.1 in Fig. 2(a). In Fig. 2(b) the variable in the vertical axis is the local velocity u which is normalized by the velocity at the centerline u_m . The variable in the horizontal axis in Fig. 2(b) is the location of x -direction which is normalized by $b_{1/2}$ which is the position of x -direction at the velocity of $1/2u_m$. The theoretical result of Tollmien's axi-symmetric jet flow is also shown in Fig. 2(b) for comparison with the present numerical data. Both the numerical results and the Tollmien's theoretical one agree well with each other showing the decreasing radial direction velocity profiles. From these results we conclude to proceed to calculate the hydrogen jet flow problem.

a

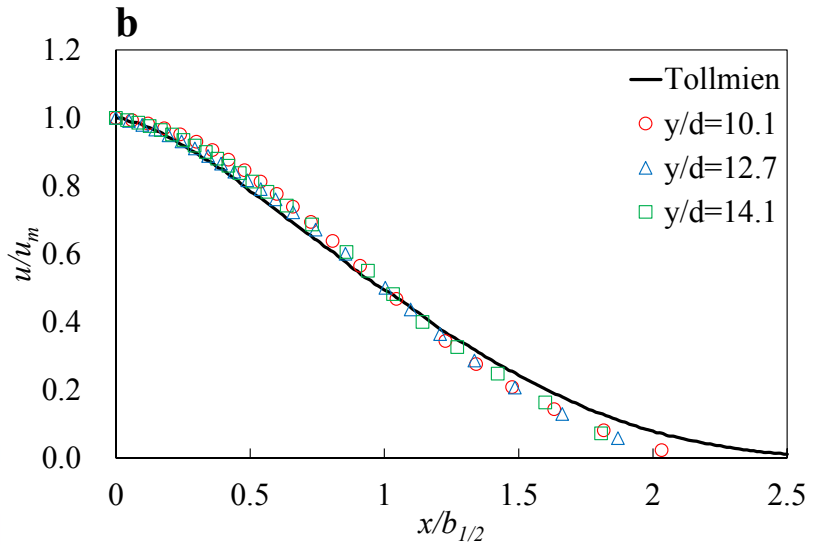
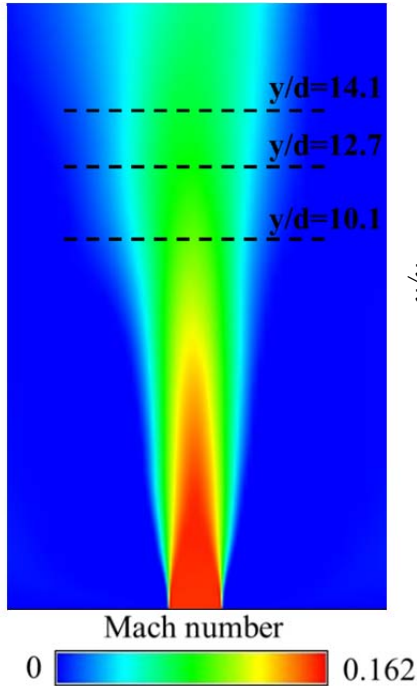


Figure 2. Average image and the comparison with the theoretical result. (a) average Mach number distribution of jet near the nozzle exit; and (b) the comparison of radial profile of non-dimensional velocity with the theoretical data of Tollmien's theory.

The comparison between the radial-direction profiles of the mean mass fraction obtained by the present numerical simulation and that by the Schefer's experiment [8] is shown in Fig. 3. The vertical axis in Fig. 3 shows the hydrogen mass fraction and the horizontal axis shows the radial

location of x which is normalized to the nozzle exit diameter. The locations of the jet flow axis y/d are picked up that which is at the closest locations in the experiments. The numerical profiles agree well with the experimental ones except for the $y/d=23.9$. On the other hand, the mass fraction profile of the numerical simulation at $y/d=23.9$ diffuse out slower than that of the Schefer's experimental results [8]. The hydrogen mass fraction is highest at the centerline near the nozzle exit and decreases toward the outside.

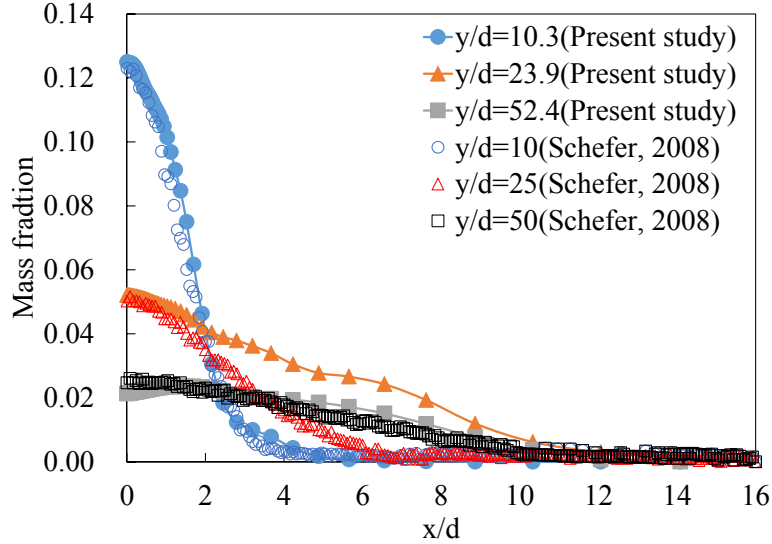


Figure 3. Comparison of radial profile of the mean mass fraction obtained by the numerical simulation with that by the present study (●, ▲, ■) and that by the Schefer's study [8] (○, △, □).

Figure 4 shows the hydrogen mole fraction profiles against the non-dimensional distance y/θ on the centerline of jets, where θ is called the equivalent diameter and is given as follows:

$$\theta = D \sqrt{\left(\frac{2}{\kappa+1}\right)^{\frac{1}{\kappa-1}} \frac{P_0 R_{air} T_a}{R_{H_2} P_a}} \quad (12)$$

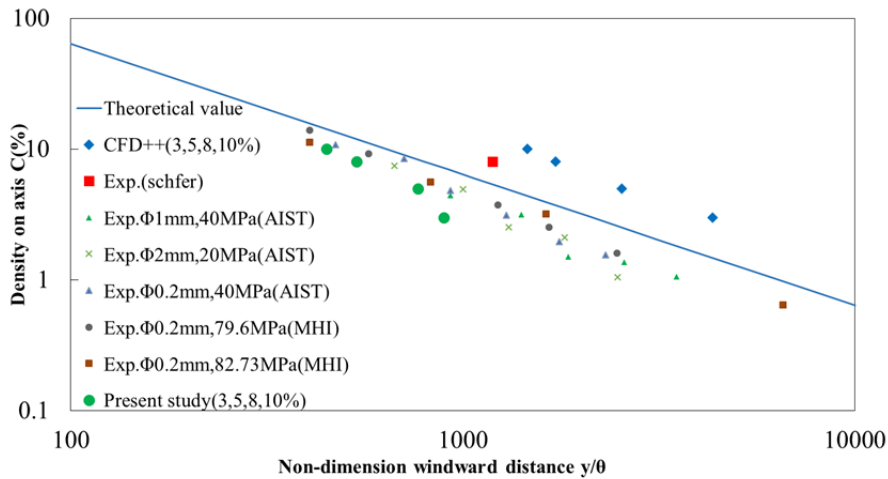


Figure 4. Hydrogen mole fraction at the centerline of jet vs. the radian distance normalized by the equivalent diameter.

where R is the gas constant of each gas. In the figure the results of the experiments by Schefer et al. [7], of the AIST [18], and MHI experiments for the high pressure hydrogen jets [4], of the CFD++ commercial program [19] to compare with the experimental results by Schefer et al. [7], and of the theoretical analysis by Tollmien are shown. The present numerical results are close to the theoretical values when the data are normalized by the equivalent diameter, and also agree well

with the experimental data. Hence from these results we conclude the present numerical simulation is validated.

5.2 Instantaneous Image of Hydrogen Jet

The instantaneous images of the properties of hydrogen jet at the time of 8.35 sec from the beginning of jetting are shown in Fig. 5, where the Mach number is shown in Fig. 5(a), pressure in Fig. 5(b), density in Fig. 5(c), and mole concentration in Fig. 5(d). In the figures the Kelvin-Helmholtz instabilities appear at the shear layer between hydrogen and air from both edges of the hydrogen jet exit to downstream. The width of the hydrogen jet becomes wider because of the instability. The pressure profiles in Fig. 5(b) shows that the high pressure region and low pressure one come out alternately by interacting each other from the nozzle exit to downstream and widen their regions as they propagate downstream. The Mach number profiles show the fluctuation of hydrogen by the interaction between the low and high pressure regions.

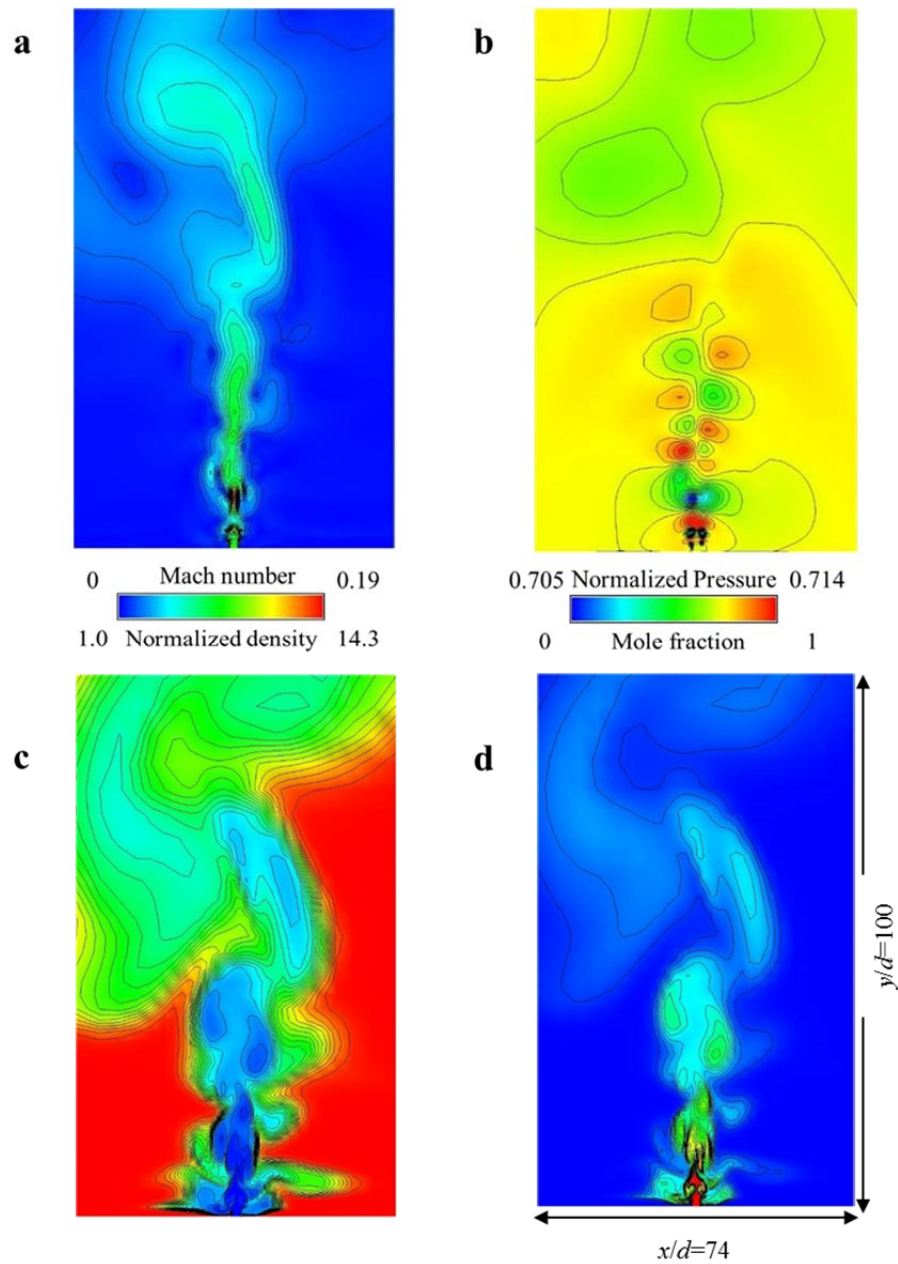


Figure 5. Instantaneous image of hydrogen jet. (a)Mach number; (b) Normalized Pressure; (c)Normalized density; and (d)Mole fraction($t=8.35$).

6.0 CONCLUSIONS

The present study performed the numerical simulation of the low speed hydrogen jet using the numerical program of the three-dimensional compressible Navier-Stokes equations with the preconditioning method. The present numerical results of hydrogen jets agree with the results using Tollmien's theory and we confirmed that the present code can simulate a general gas jet problem. The comparison of the present results with the experimental results by Schefer et al. shows that the computed mass fraction profiles along radial direction agree well with them. The normalized mole fraction agrees well with the past experimental results of the high and low pressure experimental results and shows a lower result than the theoretical ones. The results of the mole fraction using the commercial code CFD++ were found to be the larger than the present numerical data. It is confirmed that the widening of the jet width towards downstream comes from the Kelvin-Helmholtz instability. The high pressure and low pressure regions are developing alternately in the flow field and cause a fluctuation of the hydrogen jet along the pressure interaction.

ACKNOWLEDGMENTS

This research was done in collaboration with Cybermedia Center using the Osaka University supercomputer system. This study is supported by the New Energy and Industrial Technology Development Organization of Japan (NEDO) under the project "Research and Development of Technology for Hydrogen Utilization.

REFERENCES

1. Birch, A.D., Brown, D.R. and Dodson, M.G., Ignition Probabilities in Turbulent Mixing Flows, *18th International Symposium on Combustion*, 1981, pp. 1775-1780.
2. Swain, M.R., Filoso, P.A. and Swain, M.N., Ignition of lean hydrogen-air mixtures, *International Journal of Hydrogen Energy*, **30**, 2005, pp. 1447-1455.
3. Swain, M.R., Filoso, P.A. and Swain, M.N., An experimental investigation into the ignition of leaking hydrogen, *International Journal of Hydrogen Energy*, **32**, 2007, pp. 287-295.
4. Takeno, K., Okabayashi, K., Kouchi, A., Nonaka, T., Hashiguchi, K. and Chitose, K., Dispersion and explosion field tests for 40 MPa pressurized hydrogen, *International Journal of Hydrogen Energy*, **32**, 2007, pp. 2144-2153.
5. Schefer, R.W., Evans, G.H., Zhang, J., Ruggles, A.J. and Greif, R., Ignitability limits for combustion of unintended hydrogen releases: Experimental and theoretical results, *International Journal of Hydrogen Energy*, **36**, 2011, pp. 2426-2435.
6. Schefer, R.W., Houf, W.G., Williams, T.C., Bourne, B. and Colton, J., Characterization of high-pressure, underexpanded hydrogen-jet flames, *International Journal of Hydrogen Energy*, **32**, 2007, pp. 2081-2093.
7. Schefer, R.W., Houf, W.G. and Williams, T.C., Investigation of small-scale unintended releases of hydrogen: Buoyancy effects, *International Journal of Hydrogen Energy*, **33**, 2008, pp. 4702-4712.
8. Schefer, R.W., Houf, W.G. and Williams, T.C., Investigation of small-scale unintended releases of hydrogen: momentum-dominated region, *International Journal of Hydrogen Energy*, **33**, 2008, pp. 6373-6384.
9. Houf, W.G., Evans, G.H. and Schefer, R.W., Analysis of jet flames and unignited jets from unintended releases of hydrogen, *International Journal of Hydrogen Energy*, **34**, 2009, pp. 5961-5969.
10. Khaksarfard, R. and Paraschivoiu, M., Numerical simulation of high pressure hydrogen release through an expanding opening, *International Journal of Hydrogen Energy*, **37**, 2012, pp. 8734-8743.
11. Wang, C.J., Wen, J.X., Chen, Z.B. and Dembele, S., Predicting radiative characteristics of hydrogen and hydrogen/methane jet fires using FireFORM, *International Journal of Hydrogen Energy*, **39**, 2014, pp. 20560-20569.
12. Turkel, E., Preconditioned Methods for Solving the Incompressible and Low Speed Compressible Equations, *Journal of computational physics*, **72**, 1987, pp. 277-298.

13. Edwards, J.R. and Liu, M.S., Low-diffusion Flux-splitting Scheme for Flows at All Speeds, *AIAA Journal*, **36**, 1998, pp. 1610-1617.
14. Venkateswaran, S. and Merkle, C.L., Dual Time Stepping and Preconditioning for Unsteady Computations, *AIAA Journal*, **33**, 1995, 95-1673.
15. Zong, N. and Yang, V., An Efficient Preconditioning Scheme for Real-fluid Mixtures Using Primitive Pressure-temperature Variables, *International Journal of Computational Field Dynamics*, **21**, 2007, pp.217-230.
16. Weiss, J.M. and Smith, W.A., Preconditioning Applied to Variable and Constant Density Flow, *AIAA Journal*, **33**, 1995, pp. 2050-2057.
17. Edwards, J.R., Franklin, R.K. and Liu, M.S., Low-diffusion Flux splitting Methods for Real Fluid Flows with Phase Transitions, *AIAA Journal*, **38**, 2000, pp. 1624-1633.
18. Investigation on hydrogen network development: Safety technology of conductor, Report on study of hydrogen leak/diffusion behaviours, National Institute of Advanced Industrial, Science, and Technology, 2011.
19. CFD++ code, Metacomp Technologies Inc., <http://www.metacomptech.com/>.